Comparison of optical coherence tomography, microcomputed tomography, and histology at a three-dimensionally imaged trabecular bone sample

Christoph Kasseck
Ruhr-University Bochum
Photonics and Terahertz Technology
Universitaetsstrasse 150
44780 Bochum, Germany

Marita Kratz
Philipps University, Marburg
Experimental Orthopaedics and Biomechanics
Baldingerstrasse
35043 Marburg, Germany

Antonia Torcasio
Katholieke Universiteit Leuven
Division of Biomechanics and Engineering Design
Celestijnenlaan 300c
3001 Leuven, Belgium

Nils C. Gerhardt
Ruhr-University Bochum
Photonics and Terahertz Technology
Universitaetsstrasse 150
44780 Bochum, Germany

G. Harry van Lenthe
Katholieke Universiteit Leuven
Division of Biomechanics and Engineering Design
Celestijnenlaan 300c
3001 Leuven, Belgium

Thilo Gambichler
Klaus Hoffmann
St. Josef Hospital
Department of Dermatology and Allergology
Gudrunstrasse 56
44791 Bochum, Germany

David B. Jones
Philipps University, Marburg
Experimental Orthopaedics and Biomechanics
Baldingerstrasse
35043 Marburg, Germany

Martin R. Hofmann
Ruhr-University Bochum
Photonics and Terahertz Technology
Universitaetsstrasse 150
44780 Bochum, Germany

Address all correspondence to Nils C. Gerhardt, Photonics and Terahertz Technology, Ruhr-University Bochum, Universitaetsstr. 150, 44780 Bochum, Germany. Tel: 49-234-32-26514; Fax: 49-234-32-14167; E-mail: E-mail: nils.gerhardt@rub.de

Abstract. We investigate optical coherence tomography (OCT) as a method for imaging bone. The OCT images are compared directly to those of the standard methods of bone histology and microcomputed tomography (μCT) on a single, fixed human femoral trabecular bone sample. An advantage of OCT over bone histology is its noninvasive nature. OCT also images the lamellar structure of trabeculae at slightly higher contrast than normal bone histology. While μCT visualizes the trabecular framework of the whole sample, OCT can image additionally cells with a penetration depth limited approximately to 1 mm. The most significant advantage of OCT, however, is the absence of toxic effects (no ionizing radiation), i.e., continuous images may be made and individual cell tracking may be performed. The penetration depth of OCT, however, limits its use to small animal models and small bone organ cultures. © *2010 Society of Photo-Optical Instrumentation Engineers.* [DOI: 10.1117/1.3477193]

1 Introduction

Imaging of the fine structure of bone, especially trabecular bone, is important to understand the processes of bone formation and resorption.[1–4] This knowledge might help to investigate osteoporosis, for example,[1,2] or bone-invading tumors.[3,4] Presently, bone structure is investigated using mainly two standard methods, namely bone histomorphometry/histochemistry (histology) and microcomputed tomography (μCT).[5,6] Small animal (rats and mice) and bone culturing systems have been developed for the purpose of investigation of a wide variety of processes in metabolic bone.[7–10] They keep bone samples in a metabolic state for several weeks, allowing the monitoring of these processes. In particular, the interaction between continuous bone growth and resorption in the marrow region can be observed in culture chambers,[8] which is inherently a critical requirement for investigation of osteoporotic or cancerous processes.

Furthermore, dedicated culture chambers, such as the ZETOS,[8,11] offer the possibility of applying particular forces onto the bone that could, e.g., simulate natural loading forces onto the bone. These forces can be varied regarding frequency, amplitude, and direction, and they stimulate a bone growth reaction in existing bone.[12] The trabecular bone consists of a solid framework of small bone girders as struts and/or plates, called trabeculae. The single trabeculae are covered by bone lining cells and surrounded by bone marrow

cells.[13,14] However, the average thickness of trabeculae, the average density of single trabeculae (mineralization density), and the bone framework (macro architecture) density are important parameters, which influence the total bone strength and therefore have to be observed for investigations regarding, e.g., osteoporosis.[15–17] For analyzing bone growth processes in long-time studies, an appropriate tomographic method has to be used, which should provide three-dimensional, high-resolution, and *in vitro* imaging of bone samples.

A very well accepted imaging technique for monitoring bone structure *in vitro/ex vivo* is μCT.[18–24] It provides imaging capabilities with isotropic resolutions ranging from a few millimeters (clinical CT), down to few micrometers (μCT), and even further down to a hundred nanometers with synchrotron radiation sources (nanoCT). Desktop μCT is a precise and validated technique and has been used extensively for different research projects involving bone cultures,[18] small animal bones,[19–21] and trabecular bone specimens from larger animals and humans.[22,23] However, it uses ionizing x rays for imaging.

In contrast, optical coherence tomography (OCT) is a nonionizing imaging method. Furthermore, it is an approved method to generate high-resolution, contactless, tomographic images of biological samples.[24,25] Thus, OCT is exactly matched to the specifications for observing bone growth processes within a bone culturing chamber. However, up to now, bone samples have been investigated with OCT rather sparsely,[26–30] and the conditions for the applicability of OCT for monitoring bone growth are rather undefined.

In this paper, we analyze the potential of OCT for imaging of a human trabecular bone sample. For validation, the OCT images are directly compared with the corresponding μCT and histology images from the same sample position. Such a validation of OCT imaging of trabecular bone has not been reported up to now, to our knowledge. This paper is organized as follows: In Sec. 2, the sample preparation, both imaging systems, and the histology procedure are described. The μCT images are compared regarding visualization of the trabecular framework to the OCT images in Sec. 3. Direct comparison of the histology, OCT, and μCT is found in Sec. 4, and the conclusion is given in Sec. 5.

2 Sample Preparation, Imaging Systems, Histology Procedure

The bone samples were extracted from total hip bone replacements of patients with coxarthrosis. Mandatory patient agreement and confirmation by the ethics commission were secured. The bone was kept in a sterile 0.9% sodium chloride solution at 4 to 6 °C, to limit the amount of damage caused by heat and to stop the bone from drying out during all cutting procedures. For fixation, the bones were kept in 70% ethanol, stored at 4 to 6 °C, and last iteratively dehydrated with ethanol. Xylene was used for degreasing as a preparation step for polymerization with Technovit 9100. The samples were afterward cut into cubes of about $4 \times 3 \times 4$ mm (width x height x length), and a grid line structure was scratched onto their surfaces. Equidistant vertical (500 μm) and horizontal lines (200 μm) and a labeled corner facilitate imaging navigation during the different measurements. Accurate mapping was
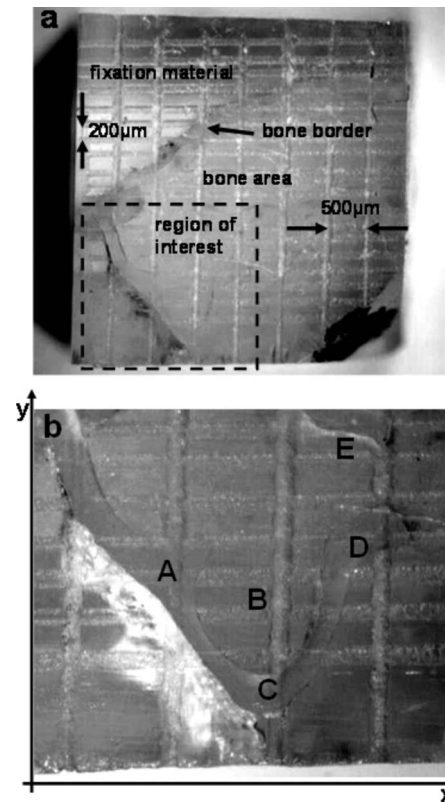

Fig. 1 Surface microscopies (x-y plane) of the sample: (a) image of the whole sample surface of about 4 mm $\times$ 4 mm, and (b) zoomed microscopic view (2 mm $\times$ 2 mm) of the region of interest (ROI), with structures labeled A to E.

performed with surface microscopy as well, with a 3-D overview image acquired by μCT. The sample surface, which passed all four imaging methods, is visualized in Fig. 1 by microscopy.

Figures 1(a) and 1(b) show the grid lines at the surface of the sample. Figure 1(b) is the zoomed microscopic view of the region of interest (ROI) from Fig. 1(a), containing a specific trabecular bone structure. This area is imaged with μCT as well as with OCT and last investigated with histology. The three-dimensional data sets of μCT and OCT of this region are compared stepwise in two-dimensional images for accurate comparison. The histology images are compared to the OCT images for evaluation of the imaging capability of OCT in the last step.

With the SkinDex300 system from Isis Optronics (Mannheim, Germany), OCT images with an axial resolution of 5 μm in tissue and with a lateral resolution of 6 μm were acquired. This is a time domain OCT system with dynamic focusing using a superluminescence diode (SLD) with a center wavelength of 1300 nm and a bandwidth of 100 nm (FWHM). The system operates in an eight-channel acquisition mode, resulting in a frame speed of about 10 frames/min. The frames have a width of 1.0 mm and a height of 0.9 mm. An additionally implemented micrometer sample positioner in the x direction [Fig. 1(b)] provides a third scanning range for subsequent frames and therefore for three-dimensional imaging. These subsequent images were recorded in 20-μm steps

over a length of 1.6 mm, resulting in a cuboidal data set of 81 images. In this paper, we compare the images step by step with the μCT data in order to demonstrate the high potential of OCT for high-resolution three-dimensional bone imaging.

After the OCT measurements, the three-dimensional microstructure of the bone sample was assessed by microcomputed tomography (Skyscan 1172, Skyscan, Kontich, Belgium). The sample was scanned using a 6.5-μm nominal isotropic resolution at a voltage of 60 kV and a maximum current of 140 μA. A 0.5 μm Al filter was used in order to obtain a better contrast in the x-ray shadow images and reduce beam hardening artifacts. The exposure time was 316 ms. Image calculation was performed using IPL (Image Processing Language, from Scanco Medical, Brüttisellen, Switzerland). The acquired images were visually aligned with the OCT images to obtain qualitative comparison.

Last, histology was performed on the sample. For that purpose, the sample was sliced into 4-μm thin slices, providing approximately the same lateral resolution as both imaging systems. The slices were first examined under the microscope in an unstained state and subsequently with van-Kossa/Giemsa staining. These images were again directly compared with the OCT images with accurate position matching.

3 Comparison of μCT with OCT

The μCT images are presented in this section, providing an overview over the whole sample and serving as an orientation. Figures 2(a) and 2(b) depict sample images obtained with μCT at different zoom factors.

Figure 2(a) visualizes the whole trabecular framework of the sample, showing the same structure details from A to E as in the microscopic image in Fig. 1(b). The continuous line in Fig. 2(b) labels the surface of the complete OCT data cuboid (1 mm $\times$ 0.9 mm $\times$ 1.6mm, W $\times$ H $\times$ L) in which the 81 OCT images were recorded. Selected OCT images within this cuboid are serially lettered from A to H and their scan position line at the surface is depicted with red dashed lines. A typical OCT image of the sample is shown in Fig. 3.

The detector glass plate and sample surface both appear as bright lines at the top of the image. The scratched equidistant vertical grid lines (500 μm between) at the sample surface are visible at the left and right as well as in the middle. Marrow cell membranes with diameters of about 70 μm are clearly visible at upper image areas, while they are at least partially identifiable at the image bottom. Marrow cells appear only weakly beyond the trabeculae, probably due to the high scattering coefficient of the bone material. However, trabeculae themselves and even inner structures of them (lamellar structure) are uncovered over the complete imaging range.

Figures 4(a)–4(h) illustrate a sequence of OCT images of the OCT data cuboid. The OCT images (blue scaled) are directly matched to the corresponding μCT images (gray scaled), allowing an accurate comparison regarding image quality of both imaging systems.

Obviously, both methods demonstrate a very high correlation in visualizing position and thickness of trabeculae. This allows a determination of the average trabecular thickness as well as the density of the trabecular framework in both cases. But in contrast to OCT, μCT does not visualize cell mem-
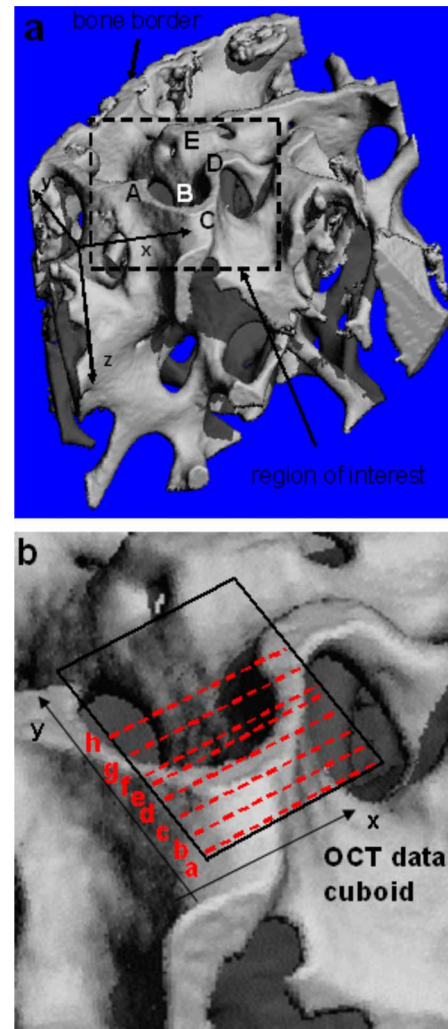

Fig. 2 Bone sample imaged with μCT: (a) complete bone sample (4 mm $\times$ 3 mm $\times$ 4 mm), with structures from Fig. 1(b), and (b) zoom into ROI with selected OCT image scan positions (red dashed lines) lettered alphabetically from the whole OCT data cuboid (black solid lines). All lines are within the surface plane (x-y plane). (Color online only.)

branes, probably due to the too low x-ray absorption coefficient of soft tissue.

Furthermore, OCT shows signal variations within the bone tissue, which most probably result from the lamellar structure of the trabeculae. However, the comparison with μCT does not validate this assumption, because the μCT images do not show these structures. The following section therefore compares these lamellar bone structures of the OCT images with the corresponding histological images for further evaluation.

4 Comparison of OCT with Histology

In Figs. 5 and 6, a histology image is directly compared to the corresponding OCT and μCT images. In the cases of unstained histology (a) and OCT (b) in Fig. 5, lamellar structures of the trabeculae are clearly visible, while they are not visible within the μCT image. The histological image therefore validates the image details of the OCT image within the trabeculae.
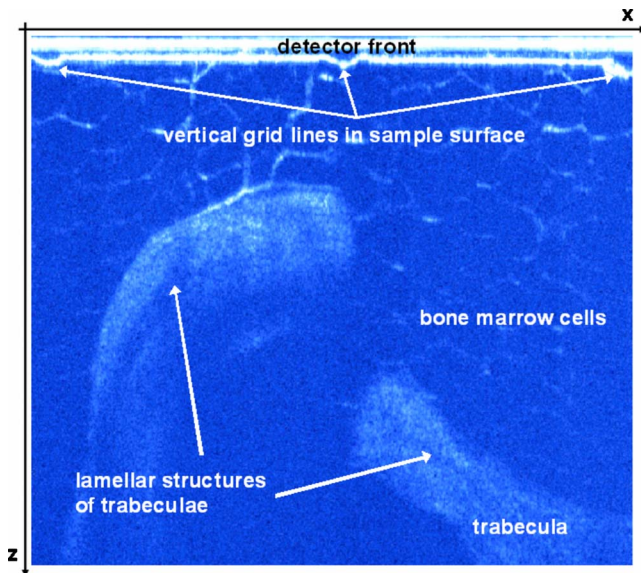
Fig. 3 Typical OCT image (1.0-mm width ×0.9-mm height) of the human bone sample.

Furthermore, the marrow cells are not visible in unstained histological slices. OCT, in contrast, clearly visualizes their honeycomb-shaped membranes in Fig. 5(b) on the right. For further cell investigation via histology, cells can be visualized by the Van-Kossa/Giemsa staining. A histological slice stained with the Van-Kossa/Giemsa method is shown in Fig. 6(a). Silver is used in the Van-Kossa/Giemsa staining as contrast agent, which strongly increases the visibility of the marrow cells and of the mineralized tissue [Fig. 6(a)]. Unfortunately, this staining method leads to the total loss of information about lamellar bone structures, which are in contrast again clearly visible in the OCT image in Fig. 6(b). Cells and lamellar structure may be uncovered synchronously with the appro-
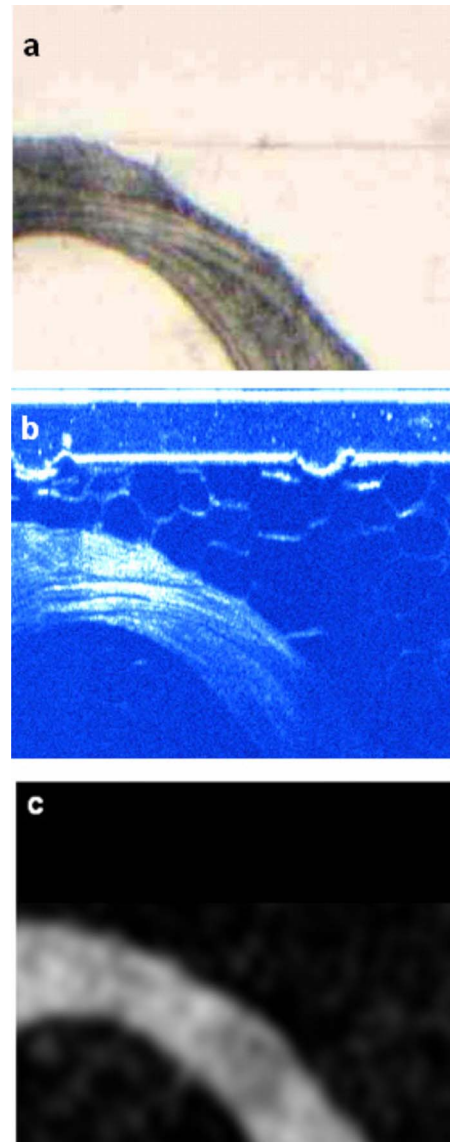

Fig. 5 Comparison of unstained histology with an OCT image of trabeculae with inner bone structures: (a) unstained histology, (b) corresponding OCT image, and (c) corresponding μCT image. Image dimensions: 0.7 mm×0.5 mm (W×H).

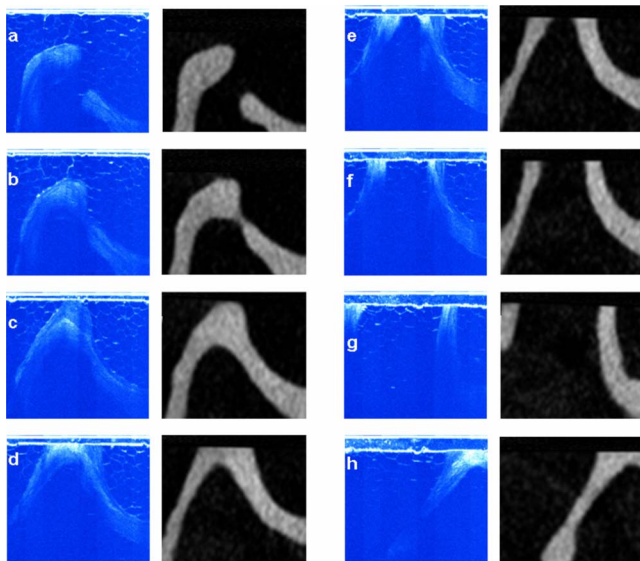priate choice of staining agent, e.g., with toluidine blue.[31] For comparison purposes, the corresponding μCT image is presented in Fig. 6(c), visualizing only the shape of the trabecula.

5 Discussion and Conclusion

OCT and μCT demonstrate a high correlation in visualizing trabecular architecture of fixated human bone samples. The μCT system is capable of imaging deeper-lying structures, while the OCT system offers more contrast and therefore more image details than μCT of hard and soft tissue at comparable nominal resolutions (5 μm×6 μm versus 6.5 μm ×6.5 μm, depth x lateral). OCT uncovers marrow cell membranes and lamellar bone structures. These image details were verified with unstained and stained histology. At surface-near positions of OCT images, the lamellar structure of trabeculae
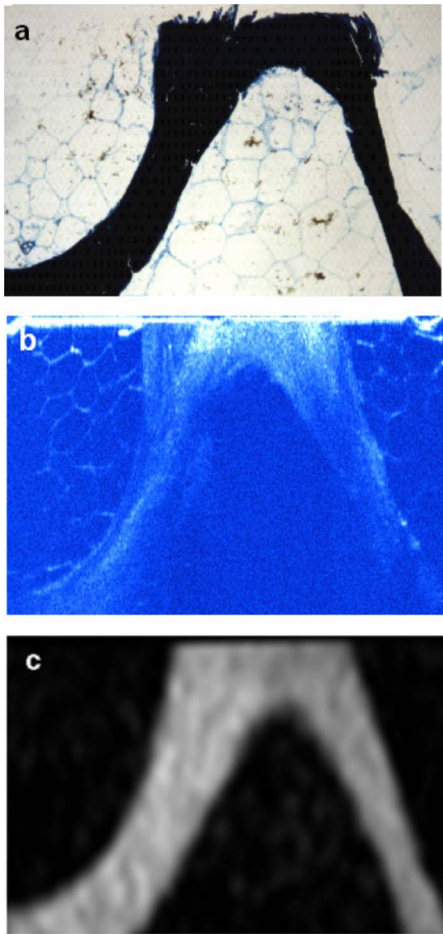

Fig. 4 (a) to (h): OCT image sequence (blue scaled) compared to μCT (gray scaled). Image dimensions: 1.0 mm×0.9 mm (W×H). (Color online only.)

Fig. 6 Comparison of stained histology with an OCT image of a trabecula with inner bone structures: (a) van-Kossa/Giemsa-stained histology, (b) corresponding OCT image, and (c) corresponding μCT image. Image dimensions: 1.0 mm×0.9 mm (W×H).

seems to show slightly higher contrast than normal bone histology. This provides a detailed monitoring of bone structure and, with extended periods of time, also a monitoring of bone growth. The imaging of cells might offer further insights of the organism activity. In particular, we anticipate the possibility of monitoring the activity of osteoclasts with OCT.

Cell membranes are soft tissue with very low x-ray attenuation compared to bone. As a result, cells probably cannot be imaged clearly by x rays. The bone lamellae, which can be visualized by OCT but not by μCT, demand further explanation. A closer look at the OCT and μCT systems offers two possible explanations for the lower contrast of μCT images. First, μCT visualizes mainly substance density, which is quite homogeneous in calcified tissue.[32] On a microstructural level, calcified bone tissue consists of many layers of lamellae, which contain highly directed mineralized collagen fibrils.[32] Next to providing information on the refractive index difference, standard OCT is also sensitive to the directionality of highly organized substances and thus probably also to the direction of collagen fibrils.[25,33] Based on our findings, we hypothesize that OCT is capable of imaging the lamellar structures due to their high percentage of collagen fibrils. In this respect, it is interesting that the high directionality of the

fibrils is also proposed as an explanation of the high contrast of lamellae imaged with high-frequency ultrasound.[32] Second, OCT analyzes the backscattered (reflected) light. Backscattering (reflection) is determined by Fresnels equations and thus is directly proportional to the squared refractive index difference. On the other hand, μCT contrast is mainly proportional to the density of the material.[34] Although the material density is nearly homogeneous in trabeculae, relevant changes in the squared refractive index difference still might appear and cause the contrast in OCT images.

In summary, OCT provides monitoring of cell activities of cultured, metabolic bone samples. Bone growth over extended periods of time can be observed without ionizing radiation. Due to the inherent invasive nature of extraction of trabecular bone, OCT seems to be particularly relevant for *in vitro* investigations of these samples. Bone also might be investigated *in vivo* by OCT with endoscopic equipment. But in this case, only the outer area of the cortical bone can be part of the diagnosis.

References

1. P. Roschger, P. Fratzl, K. Klaushofer, and G. Rodan, "Mineralization of cancellous bone after alendronate and sodium fluoride treatment: a quantitative backscattered electron imaging study on minipig ribs," *Bone* **20**, 393–397 (1997).
2. E. Atti, S. Gomez, S. M. Wahl, R. Mendelsohn, E. Paschalis, and A. L. Boskey, "Effects of transforming growth factor-beta deficiency on bone development: a Fourier transform–infrared imaging analysis," *Bone* **31**, 675–684 (2002).
3. V. Fritz, P. Louis-Plence, F. Apparailly, D. Noel, R. Voide, A. Pillon, J. C. Nicolas, R. Muller, and C. Jorgensen, "Micro-CT combined with bioluminescence imaging: a dynamic approach to detect early tumor–bone interaction in a tumor osteolysis murine model," *Bone* **40**, 1032–1040 (2007).
4. Z. A. Dotan, "Bone imaging in prostate cancer," *Nat. Clin. Pract. Urol.* **5**, 434–444 (2008).
5. J. S. Thomsen, A. Laib, B. Koller, S. Prohaska, L. Mosekilde, and W. Gowin, "Stereological measures of trabecular bone structure: comparison of 3-D microcomputed tomography with 2-D histological sections in human proximal tibial bone biopsies," *J. Microsc.-Oxf.* **218**, 171–179 (2005).
6. V. Cnudde, B. Masschaele, H. E. V. De Cock, K. Olstad, L. Vlaminck, J. Vlassenbroeck, M. Dierick, Y. D. Witte, L. Van Hoorebeke, and P. Jacobs "Virtual histology by means of high-resolution x-ray CT," *J. Microsc.-Oxf.* **232**, 476–485 (2008).
7. P. Goldhabe, "Tissue culture of bone as a model system for periodontal research," *J. Dent. Res.* **50**, 278–285 (1971).
8. C. M. Davies, D. B. Jones, M. J. Stoddart, K. Koller, E. Smith, C. W. Archer, and R. G. Richards, "Mechanically loaded *ex vivo* bone culture system 'Zetos': systems and culture preparation," *Eur. Cells Mater* **11**, 57–75 (2006).
9. Y. C. Wang, T. Uemura, R. Dong, H. Kojima, J. Tanaka, and T. Tateishi, "Application of perfusion culture system improves *in vitro* and *in vivo* osteogenesis of bone marrow–derived osteoblastic cells in porous ceramic materials," *Tissue Eng.* **9**, 1205–1214 (2003).
10. E. Tsiridis, N. Gurav, G. Bailey, R. Sambrook, and L. Di Silvio, "A novel *ex vivo* culture system for studying bone repair," *Injury* **37**, S10–S17 (2006).
11. V. David, A. Guignandon, A. Martin, L. Malaval, M. H. Lafage-Proust, A. Rattner, V. Mann, B. Noble, D. B. Jones, and L. Vico, "*Ex vivo* bone formation in bovine trabecular bone cultured in a dynamic 3-D bioreactor is enhanced by compressive mechanical strain," *Tissue Eng. Part A* **14**(1), 117–126 (2008).
12. A. Hawkey, "Low-magnitude, high-frequency signals could reduce

bone loss during spaceflight," *J. Br. Interplanet. Soc.* **60**, 278–284 (2007).

13. S. Weiner and H. D. Wagner, "The material bone: structure mechanical function relations," *Annu. Rev. Mater. Sci.* **28**, 271–298 (1998).

14. J. Y. Rho, L. Kuhn-Spearing, and P. Zioupos, "Mechanical properties and the hierarchical structure of bone," *Med. Eng. Phys.* **20**, 92–102 (1998).

15. R. W. McCalden, J. A. McGeough, and C. M. CourtBrown, "Age-related changes in the compressive strength of cancellous bone—the relative importance of changes in density and trabecular architecture," *J. Bone Jt. Surg., Am. Vol.* **79A**, 421–427 (1997).

16. V. Shen, X. Y. Meng, X. G. Liang, R. Birchman, D. D. Wu, R. Lindsay, and D. W. Dempster, "Increased trabecular thickness without an accompanying increase in trabecular plate number or connectivity can completely restore cancellous bone strength in estrogen deficient rats," *J. Bone Miner. Res.* **10**, S356–S356 (1995).

17. M. Stenstrom, B. Olander, D. Lehto-Axtelius, J. E. Madsen, L. Nordsletten, and G. A. Carlsson, "Bone mineral density and bone structure parameters as predictors of bone strength: an analysis using computerized microtomography and gastrectomy-induced osteopenia in the rat," *J. Biomech.* **33**, 289–297 (2000).

18. G. H. van Lenthe, H. Hagenmüller, M. Bohner, S. J. Hollister, L. Meinel, and R. Müller, "Nondestructive microcomputed tomography for biological imaging and quantification of scaffold-bone interaction *in vivo*," *Biomaterials* **28**, 2479–2490 (2007).

19. T. Yamashita, Y. Nabeshima, and M. Noda, "High-resolution microcomputed tomography analyses of the abnormal trabecular bone structures in klotho gene mutant mice," *J. Endocrinol.* **164**, 239–245 (2000).

20. J. M. Alexander, I. Bab, S. Fish, R. Müller, T. Uchiyama, G. Gronowicz, M. Nahounou, Q. Zhao, D. W. White, M. Chorev, D. Gazit, and M. Rosenblatt, "Human parathyroid hormone 1-34 reverses bone loss in ovariectomized mice," *J. Bone Miner. Res.* **16**, 1665–1673 (2001).

21. C. H. Turner, Y. F. Hsieh, R. Müller, M. L. Bouxsein, D. J. Baylink, C. J. Rosen, M. D. Grynpas, L. R. Donahue, and W. G. Beamer, "Genetic regulation of cortical and trabecular bone strength and microstructure in inbred strains of mice," *J. Bone Miner. Res.* **15**, 1126–1131 (2000).

22. D. W. Dempster, F. Cosman, E. S. Kurland, H. Zhou, J. Nieves, L. Woelfert, E. Shane, K. Plavetic, R. Muller, J. Bilezikian, and R. Lindsay, "Effects of daily treatment with parathyroid hormone on bone microarchitecture and turnover in patients with osteoporosis: a paired biopsy study," *J. Bone Miner. Res.* **16**, 1846–1853 (2001).

23. R. Müller, M. Hahn, M. Vogel, G. Delling, and P. Rüegsegger, "Morphometric analysis of noninvasively assessed bone biopsies: comparison of high-resolution computed tomography and histologic sections," *Bone* **18**, 215–220 (1996).

24. B. E. Bouma and G. J. Tearney, Eds., *Handbook of Optical Coherence Tomography*, Dekker, New York (2002).

25. W. Drexler and J. G. Fujimoto, Eds., *Optical Coherence Tomography—Technology and Applications*, Springer, Berlin (2008).

26. X. Q. Xu, R. K. K. Wang, and A. El Haj, "Investigation of changes in optical attenuation of bone and neuronal cells in organ culture or three-dimensional constructs *in vitro* with optical coherence tomography: relevance to cytochrome oxidase monitoring," *Eur. Biophys. J. Biophys.* **32**, 355–362 (2003).

27. H. W. Pau, E. Lankenau, T. Just, and G. Hüttmann, "Imaging of cochlear structures by optical coherence tomography (OCT)—temporal bone experiments for an OCT-guided cochleostomy technique," *Laryngo-Rhino-Otol.* **87**, 641–646 (2008).

28. S. Antonie, C. Sinescu, M. Negrutiu, C. Sticlaru, R. Negru, P. L. Laissue, M. Rominu, and A. G. Podoleanu, "Investigation of implant bone interface with noninvasive methods: numerical simulation, strain gauges, and optical coherence tomography," in *Advances in Strength of Materials*, *Key Eng. Mater.* **399**, 193–198 (2009).

29. Z. L. Zhan, X. Z. Zhang, Q. Ye, and S. S. Xie, "Measurement of crater geometries after laser ablation of bone tissue with optical coherence tomography," *Chin. Opt. Lett.* **6**, 896–898 (2008).

30. N. Ugryumova, J. Stevens-Smith, A. Scutt, and S. J. Matcher, "Local variations in bone mineral density: a comparison of OCT versus x-ray micro-CT," *Proc. SPIE* **6847**, 684725 (2008).

31. M. D. Morris, N. J. Crane, L. E. Gomez, and M. A. Ignelzi, "Compatibility of staining protocols for bone tissue with Raman imaging," *Calcif. Tissue Int.* **74**, 86–94 (2004).

32. K. Raum, "Microelastic imaging of bone," *IEEE Trans. Ultrason. Ferroelectr. Freq. Control* **55**, 1417–1431 (2008).

33. B. H. Park, C. Saxer, S. M. Srinivas, J. S. Nelson, and J. F. de Boer, "*In vivo* burn depth determination by high-speed fiber-based polarization sensitive optical coherence tomography," *J. Biomed. Opt.* **6**, 474–479 (2001).

34. M. Stauber and R. Müller, "Microcomputed tomography—a method for the non-destructive evaluation of the three-dimensional structure of biological specimens," *Methods Mol. Biol.* **455**, 273–292 (2008).